A&A 446, 1129–1138 (2006)
DOI: 10.1051/0004-6361:20053213

Astronomy & Astrophysics

Photospheric and chromospheric active regions on three single-lined RS CVn binaries⋆

K. Biazzo[1], A. Frasca[2], S. Catalano[2], and E. Marilli[2]

[1] Department of Physics and Astronomy, University of Catania, via S. Sofia 78, 95123 Catania, Italy
e-mail: kbiazzo@ct.astro.it
[2] INAF - Catania Astrophysical Observatory, via S. Sofia 78, 95123 Catania, Italy

Received 8 April 2005 / Accepted 5 October 2005

ABSTRACT

A monitoring of three active RS CVn binaries has been performed with medium resolution spectroscopy with the aim of investigating the behavior of chromospheric and photospheric inhomogeneities. Surface temperature, as recovered from line-depth ratios (LDRs), allowed us to map the photospheric spots, while the Hα emission has been used as an indicator of chromospheric inhomogeneities. We have found that the rotational modulation of the Hα emission is always in anti-phase with the temperature wave, i.e. at the time of our observations active regions at chromospheric and photospheric levels are closely spatially associated in these active stars. The residual Hα profiles, obtained as the difference between the observed spectra and non-active templates, are well reproduced by a two Gaussian fitting. The broad emission component, responsible for the wide emission wings in near all the spectra, is often blue-shifted with respect to the center of the stellar disk. The narrow Hα emission displays a phase-dependent variation in all stars and is anti-correlated with the photospheric diagnostics, while the broad one displays no or little rotational modulation. We suggest that the broad emission component is mainly related to physical phenomena, like micro-flaring or strong chromospheric velocity fields, occurring all over the star disk, while the central narrow emission is more affected by chromospheric plages. We have also detected a modulation of the intensity of the He I D_3 line with the star rotation, suggesting surface features also in the upper chromosphere of these stars.

Key words. stars: activity – stars: starspots – stars: individual: VY Ari – stars: individual: HK Lac – stars: individual: IM Peg – techniques: spectroscopic – stars: binaries: close

1. Introduction

In late-type active stars, the rotational modulation of brightness is commonly attributed to an uneven distribution of starspots on their photospheres. Further diagnostics of photospheric activity, like Zeeman broadening/splitting of spectral lines, Doppler Imaging (DI), line-depth ratio (LDR) modulation, have been more and more frequently used in the last decade. In the meantime, several studies have demonstrated the effectiveness of the Hα line as diagnostics of chromospheric surface features (e.g. Strassmeier et al. 1993a; Catalano et al. 1996, 2000; Frasca et al. 1998, 2000a).

The simultaneous study of photospheric (spots) and chromospheric (plages) active regions (ARs) is important for a better understanding of the physical processes occurring during the emersion of magnetic flux tubes from the sub-photospheric convective level. Indeed, the relative position and size of ARs at different atmospheric levels can provide information about the magnetic field topology. In many active RS CVn binaries, rotational modulation due to surface inhomogeneities at photospheric and chromospheric level has been revealed (Frasca et al. 1998; Catalano et al. 2002).

Simultaneous photometric and spectroscopic observations have frequently shown a spatial association between spots and plages in RS CVn systems (Rodonò et al. 1987; Catalano et al. 1996; Frasca et al. 1998) as well as in young mildly-active solar-type stars (Frasca et al. 2000a; Biazzo et al. 2005). A close plage-spot association has been also detected in very active main-sequence single stars, like the rapidly rotating star LQ Hya (Strassmeier et al. 1993a). There are evidences of spot-plage associations also in close binary systems (e.g. TZ CrB, Frasca et al. 1997) and in extremely active stars, like the components of the contact binary VW Cep (Frasca et al. 1996). Moreover, for some RS CVn binary systems there are indications of a systematic longitude lag of 30°–50° between the plages and spots (Catalano et al. 1996, 2000).

In a recent paper (Catalano et al. 2002, hereafter Paper I), we presented the results of a spectroscopic monitoring of the photospheric temperature in three active single-lined RS CVn binaries, namely VY Ari, IM Peg and HK Lac, using LDRs as

⋆ Based on observations collected at Catania Astrophysical Observatory, Italy.

temperature diagnostics. In a subsequent paper (Frasca et al. 2005, hereafter Paper II), we have shown that it is possible to solve for accurate spot temperature and size by applying a spot model to contemporaneous temperature and light curves.

In the present paper, a simultaneous study of photospheric and chromospheric surface structures of these three RS CVn binaries is presented. The photospheric inhomogeneities have been detected by means of LDR modulation and light curves (Paper II), while the net Hα emission measured in the same spectra allows us to study the chromospheric structures simultaneously to the photospheric ones. The aim of the present work is to have a better comprehension of the source and location of the excess Hα emission and to give elements for the spatial association between surface inhomogeneities at different atmospheric levels.

2. Observations, reduction and data analysis

Spectroscopic observations have been performed in 2000 and 2001 at the *M. G. Fracastoro station* (Serra La Nave, Mt. Etna) of Catania Astrophysical Observatory with FRESCO (Fiber-optic Reosc Echelle Spectrograph of Catania Observatory), the échelle spectrograph connected to the 91-cm telescope through a fiber link. The spectral resolution was $R = \lambda/\Delta\lambda \simeq 14\,000$, with a 2.6-pixel sampling.

The data reduction was performed by using the ECHELLE task of the IRAF[1] package following the standard steps.

Many more details about the instrumentation and the data reduction can be found in Paper I.

2.1. Hα line analysis

It has been widely shown, both from observational and theoretical points of view, that the Hα line is a good and easily accessible diagnostics of solar and stellar chromospheric emission. Though only very active and cool stars display a pure Hα emission profile, a comparison with synthetic spectra without chromospheres or with spectra of low-activity standard stars reveals an emission contribution filling in the Hα core also for stars with a moderate activity level (see e.g. Herbig 1985; Frasca et al. 2000a; Freire Ferrero et al. 2004).

With the aim of emphasizing and then integrating the Hα chromospheric emission component that fills in the line core, we have used the "spectral synthesis" method (Barden 1985; Frasca & Catalano 1994; Montes et al. 1995), simulating the Hα photospheric profile with a well-exposed spectrum of a standard star with a negligible activity. The adopted standard star has a spectral type as close as possible to the active star to be reproduced and a low rotational velocity.

We have cleaned the spectra of the targets and standard stars from the H_2O telluric absorption lines. From spectra of fast rotating A-type stars, we produced templates suitable for the telluric H_2O line removal in the Hα region, as described in Frasca et al. (2000a).

Since the RS CVn binaries studied in the present work are single-lined systems, we used only one standard star spectrum to reproduce the observed spectra of each system. To mimic the active star in absence of chromospheric activity the standard star spectrum has been rotationally broadened by means of the convolution with a rotational profile of proper $v \sin i$. The difference between the observed spectra and this "synthetic" spectrum gives, as residuals, the net Hα chromospheric emission, while all the absorption photospheric lines cancel out to a large extent (see Figs. 2, 4, 6).

The net Hα equivalent width, $EW_{\mathrm{H}\alpha}$, has been measured by integrating all the emission profiles in the residual spectra (Figs. 2, 4, 6, right panels). The error, $\Delta EW_{\mathrm{H}\alpha}$, has been evaluated determining the S/N in two windows on the right- and left-hand side of Hα in the difference spectrum and multiplying its reciprocal for the width of the integration range. Although the errors $\Delta EW_{\mathrm{H}\alpha}$ are generally a few hundredth Å, a small systematic error in $EW_{\mathrm{H}\alpha}$, due to a contamination by chromospheric emission in the Hα core of the reference stars, could be still present. However, this contribution is completely negligible for very active stars, like the RS CVn systems here investigated. More information about the spectral synthesis method can be found in Frasca & Catalano (1994).

We have also analysed the residual Hα emission profiles by means of a multiple Gaussian fitting. This technique enabled us to identify broad and narrow emission components inside the complex Hα profile, as well as extra-absorption features displayed by IM Peg. They are possibly related to different structures and physical mechanisms in the two-component modeling as proposed by Lanzafame et al. (2000) for the chromospheric emission of the V711 Tau active system. The application of this technique to the residual Hα profiles of VY Ari, IM Peg and HK Lac is shown in Fig. 1.

2.2. Helium line analysis

Because of its high excitation potential, the helium λ 5876 line enables to trace out the regions of higher temperature and excitation in solar and stellar chromospheres. Recent models seem to indicate that the primary mechanism responsible for the formation of the He I triplet is the collisional excitation and ionization by electron impact followed by recombination cascade (Lanzafame & Byrne 1995).

In the Sun, the He I D_3 line appears as an absorption feature in plages and weak flares and in emission in strong flares (e.g. Zirin 1988). In active stars, the He I D_3 line usually appears in absorption and, only in few cases such as II Peg (Montes et al. 1997), in emission. This is probably due to the high electronic temperature and/or density in the emitting region (Zirin 1988; Lanzafame & Byrne 1995). Moreover, He I emission has been also detected during strong flares in RS CVn stars like UX Ari, II Peg (Montes et al. 1997) and HR 1099 (Foing et al. 1994). The spectral subtraction technique has allowed us to clearly detect the He I D_3 line, and to measure its equivalent width, EW_{He}.

[1] IRAF is distributed by the National Optical Astronomy Observatory, which is operated by the Association of the Universities for Research in Astronomy, inc. (AURA) under cooperative agreement with the National Science Foundation.

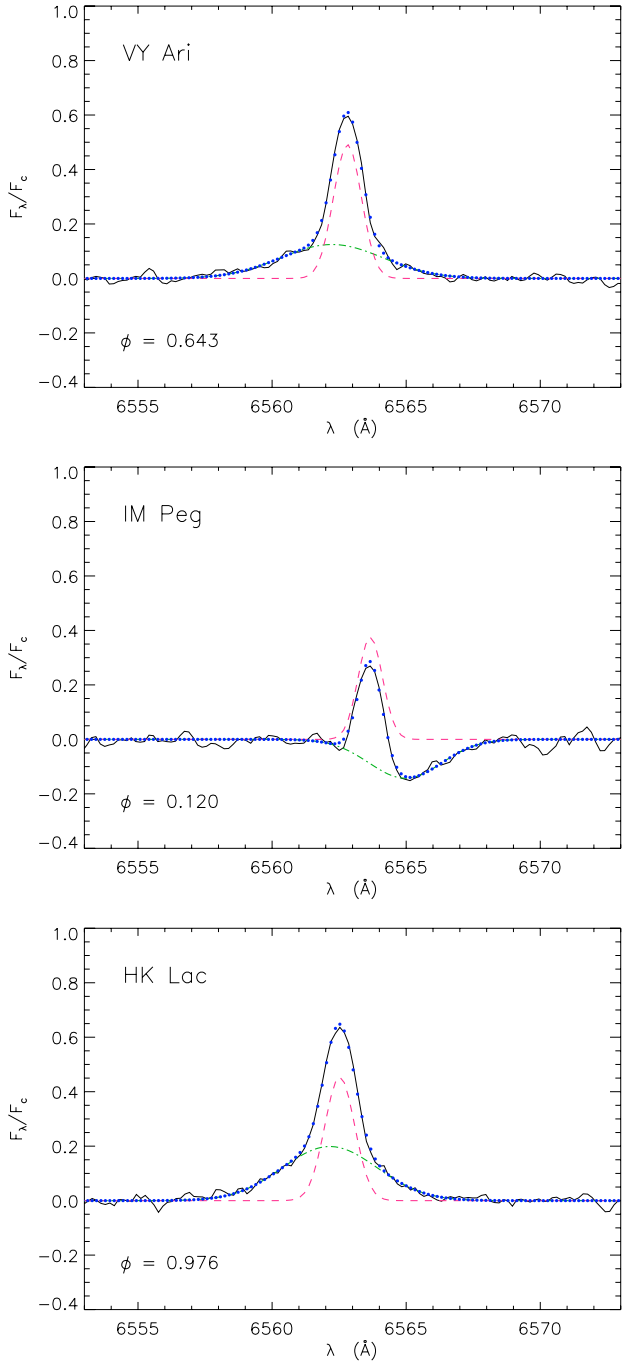

Fig. 1. Hα residual profiles (full lines) of VY Ari, IM Peg and HK Lac, from top to bottom, with two-Gaussian fits superimposed (dots). The broad and narrow Gaussian components are displayed with dash-dotted and dashed lines, respectively.

2.3. Temperature modulation from LDRs

It has been proved that line-depth ratios can be used for detecting the rotational modulation of temperature associated to cool spots in active RS CVn stars. This diagnostics allows us to resolve temperature variations as small as 10 K. The precision of this method is improved by averaging the results from several line pairs (Paper I). We have detected temperature modulations with amplitudes in the range 120–180 K for VY Ari, IM Peg and HK Lac from spectra at medium resolution (R = 14 000) that have enabled us to solve temperature and sizes of starspots (Paper II).

More information about the LDR method can be found in Paper I.

3. Results

3.1. VY Ari

We used, as non-active template for VY Ari, a spectrum of δ Eri (K0IV) convolved with a rotational profile of $v \sin i$ = 8.6 km s^{-1} (Bopp et al. 1989) and linear limb-darkening coefficient (at 6500 Å) μ_{6500} = 0.63 (Al-Naimiy 1978). The rotational phases were calculated with the ephemeris HJD$_{\phi=0}$ = 2 451 856.0 (Paper II), $P_{\rm rot}$ = 16.292 d.

Figure 2 shows a sample of spectra of VY Ari in the Hα region together with the non-active template at six different phases. The residual spectra (observed − template) are plotted in the right panels. The observed Hα profile changes from a pure double-peaked emission above the continuum level ($\phi \simeq 0\overset{\rm p}{.}22$) to a filled-in absorption ($\phi \simeq 0\overset{\rm p}{.}53$).

The values of the total emission equivalent width $EW_{\rm H\alpha}$ with their error bars are plotted in Fig. 3 as a function of the rotational phase. The temperature modulation curve and the light curve, obtained in Paper II, are also displayed in the two upper boxes of the same figure. In spite of the scatter of Hα data, a clear anti-correlation between photospheric indicators (temperature and V magnitude) and Hα emission is apparent. The maximum $EW_{\rm H\alpha}$ value of about 1.74 Å is reached at $\phi \simeq 0\overset{\rm p}{.}2$, i.e. very close to the $T_{\rm eff}$ and V minima; the minimum value of $EW_{\rm H\alpha} \simeq 0.7$ Å is observed at phase $\phi \simeq 0\overset{\rm p}{.}6$, corresponding to the $T_{\rm eff}$ and V maxima. Moreover, both curves seem to have a similar asymmetric shape. We have evaluated the significance of the $EW_{\rm H\alpha}$ modulation by means of simple χ^2 tests. In the hypothesis that the data are totally uncorrelated with the rotational phase, ϕ, one would expect no significant difference between the χ^2 values of the fit of a smooth periodic function and of a constant function (the weighted average value). We have used, as a fitting function, a Fourier polynomial of the form $f(\phi) = A + B\sin(2\pi\phi + \phi_1) + C\sin(4\pi\phi + \phi_2)$ which is able to reproduce smooth, asymmetrical curves. The reduced χ^2 of such a fit to the $EW_{\rm H\alpha}$ curve of VY Ari is 2.7, while we find a much higher value, χ^2 = 13.5, for a constant function. The probability $P_5(\chi^2)$ that a fit with 5 free parameter (like the fitting Fourier polynomial) gives a $\chi^2 \leq 2.7$ is of ≈25%, while with 1 degree of freedom, we obtain $P_1(\chi^2)$ = 99.98%, assuring the statistical significance of the observed rotational modulation.

In order to quantify the degree of anti-correlation between the photospheric and chromospheric diagnostics, we have calculated the Spearman's rank correlation coefficients by means of the IDL procedure for rank-correlation analysis R_CORRELATE (Press et al. 1986). We found a correlation coefficient ρ = 0.929 with a significance 6 × 10^{-7} for V versus $T_{\rm eff}$ curves, ρ = −0.839 with a significance 9 × 10^{-5} for V versus Hα and ρ = −0.786 with a significance 5 × 10^{-4} for $T_{\rm eff}$ versus Hα. This simple test indicates a very high degree of correlation between the two photospheric diagnostics

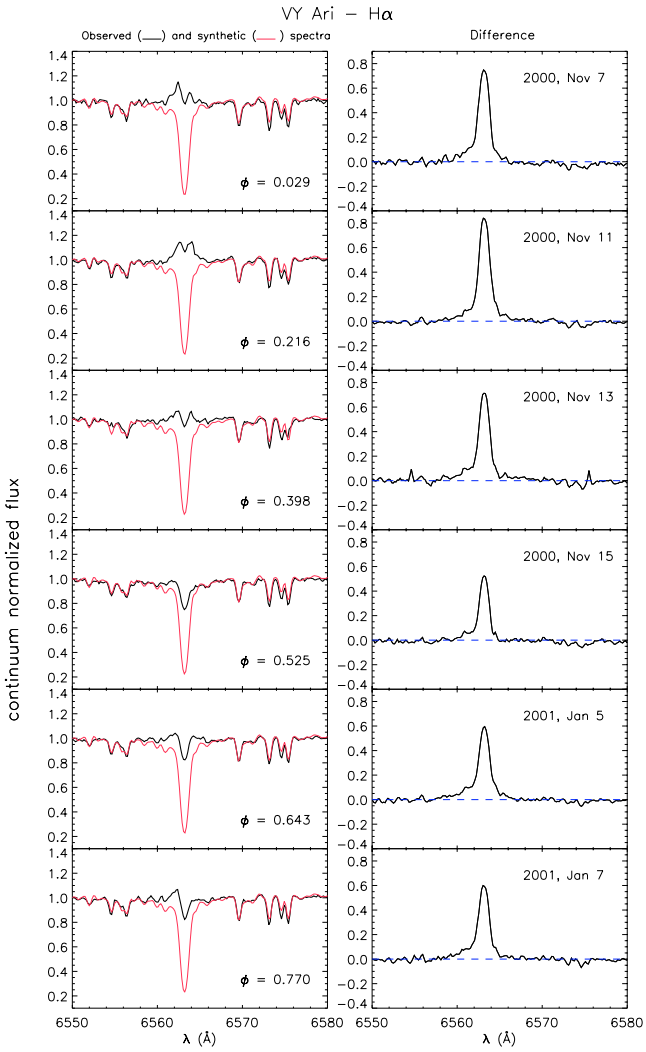

Fig. 2. *Left panels*: sample of observed and continuum-normalized spectra of VY Ari in the Hα region together with the non-active template. *Right panels*: difference between observed and template spectra.

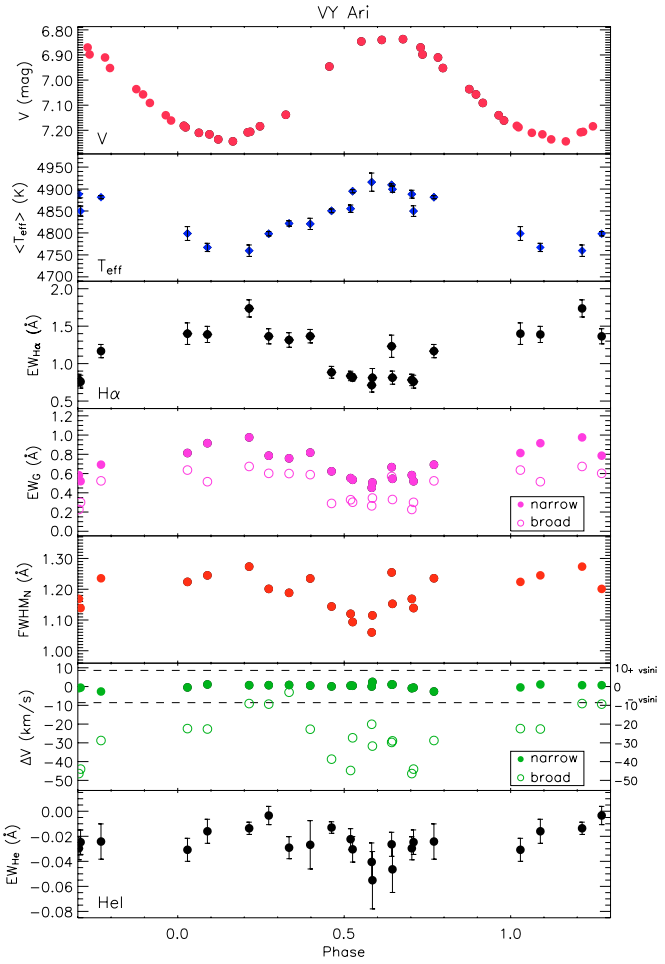

Fig. 3. *From top to bottom.* Johnson V photometry, average effective temperature, total Hα emission, equivalent width, $FWHM_{\rm N}$, relative radial velocity of the two-Gaussian fitting and He I D_3 equivalent width as a function of the rotational phase for VY Ari.

(V and $T_{\rm eff}$) and high anti-correlation between the diagnostics representative of photosphere and chromosphere. We have also applied the cross-correlation analysis in order to investigate any eventual lag between the chromospheric and photospheric flux curves. For the light curve and the Hα flux curve, we found a deep minimum of the Cross Correlation Function (CCF) of −0.88 and a phase shift of V with respect to Hα curve equal to $0\overset{p}{.}004$ that is essentially negligible, i.e the two curves are nearly exactly anti-correlated. Similar results are obtained for the $T_{\rm eff}$–Hα CCF.

The shape of the residual Hα profiles of VY Ari can be reproduced by the superposition of two emission components, a relatively narrow and a broad one. With the aim of characterizing these components we have fitted the residual Hα profiles with two Gaussians. The narrow, phase-dependent component is well fitted by a Gaussian with a $FWHM_{\rm N}$ of 50–60 km s^{-1}, while the broad one has a $FWHM_{\rm B}$ of about 120–210 km s^{-1}. The parameters of the emission components, namely integrated flux ($EW_{\rm G_{N/B}}$), $FWHM_{\rm N/B}$, and velocity shift ($\Delta V_{\rm N/B}$) with respect to the center of the stellar disk are displayed in Fig. 3 as a function of the rotational phase. The rotational modulation of the narrow emission component is clearly visible in the fourth box of Fig. 3 (dots) and displays the same trend as the total Hα emission ($EW_{\rm H\alpha}$). Though with significant scatter, the $FWHM_{\rm N}$ of this component displays a rotational modulation, with higher values near the maximum emission. This could indicate stronger velocity fields in ARs with respect to the quiet chromosphere. The centroid of the narrow component has also a radial velocity fully compatible with structures lying on the star disk, as can be seen from the ΔV values plotted in the fifth box of Fig. 3. The broad component (circles) displays a much less defined variation with phase. It is always blue-shifted, reaching values of about −50 km s^{-1} near the phase of minimum Hα emission. The equivalent width $EW_{\rm He}$ of He I D_3 line, that is always in absorption in our spectra, is also displayed in the lower box of the same figure. In spite of the data errors and scatter, the line intensity seems to be correlated with the Hα emission, with lower absorption at the phase of Hα maximum. This could be due to an eventual contribution by collisional emission dominated emission coming from denser and/or hotter plages.

Table 1. Parameters of the subtracted spectra of VY Ari.

HJD (+2 400 000)	Phase	$EW_{H\alpha}$ (Å)	$\Delta EW_{H\alpha}$ (Å)	EW_{G_N} (Å)	$FWHM_N$ (Å)	ΔV_N (km s^{-1})	EW_{G_B} (Å)	$FWHM_B$ (Å)	ΔV_B (km s^{-1})	EW_{He} (Å)	ΔEW_{He} (Å)
51 856.477	0.029	1.40	0.14	0.81	1.22	−0.5	0.64	3.51	−22.4	−0.031	0.009
51 857.453	0.089	1.39	0.11	0.92	1.25	1.1	0.52	3.17	−22.6	−0.016	0.010
51 859.496	0.215	1.74	0.11	0.98	1.27	0.7	0.67	4.07	−9.1	−0.014	0.005
51 860.453	0.273	1.36	0.10	0.79	1.20	0.7	0.60	3.28	−9.4	−0.003	0.007
51 861.449	0.334	1.32	0.10	0.76	1.19	0.8	0.60	3.58	−3.1	−0.029	0.009
51 862.484	0.398	1.37	0.09	0.82	1.23	0.5	0.59	4.28	−22.8	−0.027	0.019
51 863.527	0.462	0.88	0.08	0.62	1.14	0.1	0.29	3.13	−38.7	−0.013	0.005
51 864.559	0.525	0.82	0.05	0.54	1.09	0.4	0.30	2.88	−27.3	−0.030	0.010
51 865.492	0.583	0.71	0.09	0.45	1.06	0.0	0.26	2.84	−20.1	−0.041	0.015
51 865.527	0.585	0.81	0.12	0.51	1.12	2.5	0.35	2.63	−31.7	−0.055	0.023
51 866.508	0.645	0.81	0.09	0.55	1.15	1.1	0.33	3.11	−29.0	−0.046	0.019
51 867.539	0.708	0.76	0.09	0.52	1.14	−0.6	0.30	3.05	−44.0	−0.025	0.010
51 913.336	0.519	0.84	0.06	0.55	1.12	0.5	0.33	2.92	−44.7	−0.022	0.008
51 915.344	0.643	1.23	0.15	0.67	1.25	1.1	0.57	4.59	−29.8	−0.026	0.010
51 916.332	0.703	0.78	0.08	0.58	1.17	−0.9	0.22	3.14	−46.4	−0.030	0.009
51 917.414	0.770	1.17	0.09	0.69	1.24	−2.7	0.52	4.24	−28.8	−0.024	0.014

All the data coming from the analysis of residual spectra and displayed in Fig. 3 are listed in Table 1 for both narrow and broad components.

3.2. IM Peg

We choose a high S/N spectrum of α Ari (K2III), rotationally broadened to 25.6 km s^{-1} (De Medeiros & Mayor 1999), to produce a non-active template for IM Peg. The rotational period P_{rot} = 24.789 d (Paper II) and the initial Julian day $HJD_{\phi=0}$ = 2 443 734.0 (Strassmeier et al. 1997) were adopted for phasing the data.

The sample of observed and residual spectra of IM Peg plotted in Fig. 4 shows a filled-in variable Hα profile. On the average, this system displays an Hα activity level lower than that of VY Ari, and a pure emission Hα profile has never been observed during this season. It is worth noticing the excess absorption observed at phases from ∼0^p.1 to ∼0^p.6. This feature appears always red-shifted compared to the line center and displays a maximum intensity at $\phi \simeq 0^p.12$ when we measure an integrated residual equivalent width $EW_{H\alpha} \simeq 0$, i.e. the red-shifted extra-absorption nearly compensates the Hα emission core. Hα excess absorption has been sometimes observed in other RS CVn stars, mainly double-lined eclipsing binaries, and has been interpreted in terms of prominence-like features (e.g., Hall & Ramsey 1992; Frasca et al. 2000b).

In the third box of Fig. 5 we plot the net total Hα emission equivalent width versus rotational phase. The $EW_{H\alpha}$ data are quite scattered, but it is clear that the strongest Hα emission occurs at phases around 0^p.9, in correspondence with temperature and light curve minima. Excluding the data contaminated by extra-absorption, $EW_{H\alpha}$ ranges from about 0.3 to 0.9 Å. The reduced χ^2 of a Fourier polynomial fit to the $EW_{H\alpha}$ curve of IM Peg is 8.3, while it is 17.5, for a constant function. The probability $P_5(\chi^2)$ that a fit with 5 free parameter gives a $\chi^2 \leq 8.3$ is of about 86%, while, for the constant function (no rotational modulation), we obtain $P_1(\chi^2) \simeq 100\%$. In this case, the test cannot confirm the significance of a rotational modulation. Indeed, the $EW_{H\alpha}$ values are contaminated by the extra-absorption. Some trials made on the Hα emission core curve

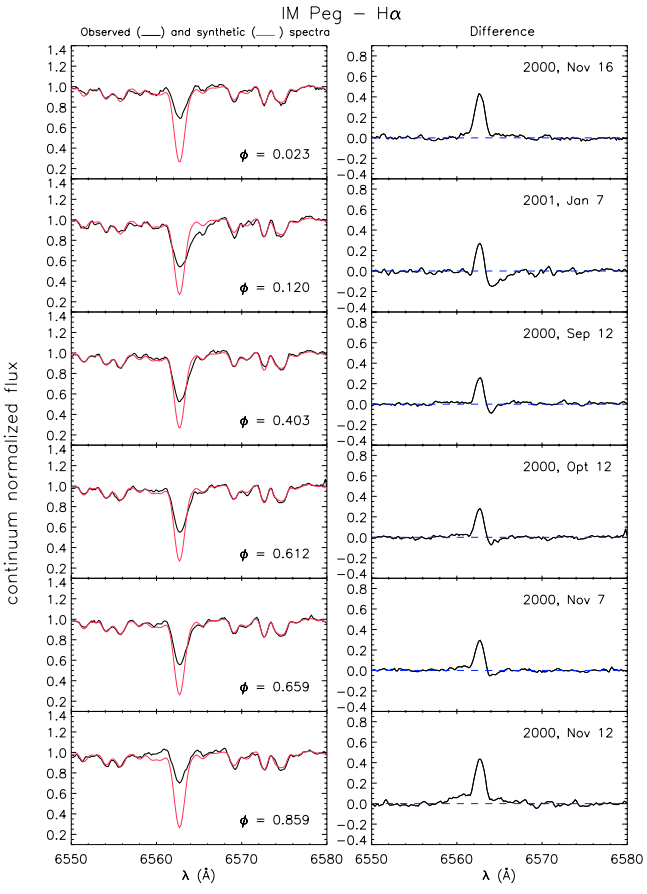

Fig. 4. *Left panels*: sample of observed and continuum-normalized spectra of IM Peg in the Hα region together with the non-active template. *Right panels*: difference between observed and template spectra.

Table 2. Parameters of the subtracted spectra of IM Peg.

HJD (+2 400 000)	Phase	$EW_{H\alpha}$ (Å)	$\Delta EW_{H\alpha}$ (Å)	EW_{G_N} (Å)	$FWHM_N$ (Å)	ΔV_N (km s^{-1})	EW_{G_B} (Å)	$FWHM_B$ (Å)	ΔV_B (km s^{-1})	EW_{He} (Å)	ΔEW_{He} (Å)
51 798.457	0.324	0.19	0.05	0.34	1.07	−1.4	−0.13	1.69	75.2	−0.099	0.024
51 800.422	0.403	0.22	0.04	0.30	1.06	−1.5	−0.09	0.97	57.5	−0.091	0.013
51 801.473	0.446	0.20	0.07	0.38	1.16	−0.1	−0.24	1.95	44.2	−0.100	0.024
51 829.430	0.573	0.35	0.09	0.34	1.10	−4.7	−0.09	1.23	75.0	−0.100	0.022
51 830.387	0.612	0.30	0.07	0.38	1.15	−1.1	−0.12	1.95	54.1	−0.102	0.025
51 831.344	0.651	0.44	0.06	0.36	1.15	−3.0	−0.06	1.12	66.8	−0.108	0.021
51 833.371	0.732	0.37	0.04	0.38	1.15	−4.6	−0.05	0.93	65.0	−0.114	0.013
51 835.395	0.814	0.40	0.05	0.46	1.26	−0.2	−0.06	1.04	55.0	−0.108	0.023
51 856.332	0.659	0.37	0.04	0.38	1.18	−1.4	−0.07	1.46	62.8	−0.121	0.021
51 859.395	0.782	0.97	0.08	0.46	1.24	−2.5	0.57	5.80	−18.3	−0.134	0.023
51 860.285	0.818	0.68	0.08	0.40	1.14	1.5	0.31	3.98	−38.1	−0.106	0.024
51 861.301	0.859	0.89	0.09	0.43	1.12	0.5	0.50	4.88	−32.9	−0.104	0.026
51 862.352	0.902	0.92	0.09	0.40	1.14	−0.1	0.54	4.89	−13.1	−0.080	0.020
51 863.363	0.942	0.51	0.05	0.46	1.16	0.6	0.07	1.85	−80.2	−0.096	0.026
51 865.352	0.023	0.65	0.04	0.50	1.19	−1.4	0.27	4.81	27.5	−0.103	0.023
51 913.258	0.955	0.71	0.06	0.50	1.20	−0.4	0.25	3.82	−86.5	−0.092	0.021
51 915.273	0.036	0.46	0.04	0.39	1.10	−2.1	0.14	3.45	−89.6	−0.083	0.025
51 917.336	0.120	−0.06	0.07	0.42	1.07	0.4	−0.48	3.16	61.0	−0.145	0.043

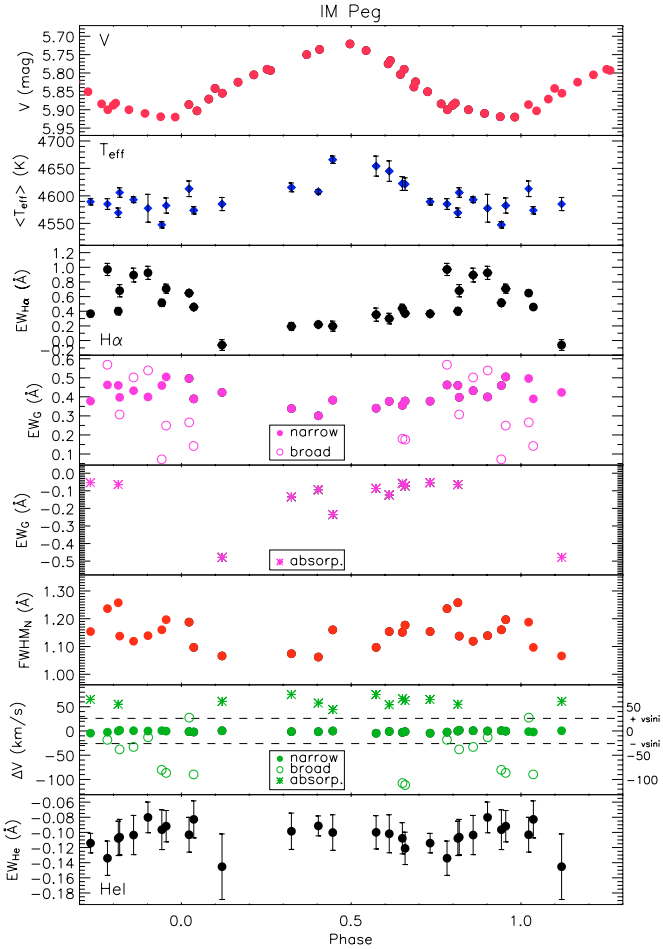

Fig. 5. *From top to bottom.* Johnson V photometry, average effective temperature, total Hα emission, equivalent width, $FWHM_N$, relative radial velocity of the two-Gaussian fitting and He I D_3 equivalent width as a function of the rotational phase for IM Peg.

provide a much higher significance of the rotational modulation, as the other systems.

As for VY Ari, we have applied the rank-correlation analysis also to the V, $T_{\rm eff}$ and Hα curves of IM Peg. The correlation coefficient was $\rho = 0.786$ with a significance 1×10^{-4} for $V - T_{\rm eff}$ correlation, $\rho = -0.845$ with a significance 1×10^{-5} for V−Hα, $\rho = -0.479$ with a significance 4×10^{-2} for $T_{\rm eff}$−Hα. These values are slightly lower than those derived for VY Ari, due to the lower amplitude of V and $T_{\rm eff}$ curves and to the influence of the extra-absorption on the Hα curve. However, a rather high degree of correlation is deduced. The cross-correlation analysis indicate a deep CCF (−0.72) with a phase shift, $\Delta\phi$, of the light curve with respect to the Hα curve of about $0\overset{\rm p}{.}07$. Given the scatter of $EW_{H\alpha}$ data, the contamination by the extra-absorption and the lower amplitude of the V and $T_{\rm eff}$ curves, this value of $\Delta\phi$ might be not considered as significant.

The residual spectra of IM Peg show a variable Hα profile with a sharp emission core, a broad blue-shifted emission component observed in the phase range $0\overset{\rm p}{.}65$–$1\overset{\rm p}{.}04$, and a red-shifted extra-absorption component in the phase range $0\overset{\rm p}{.}1$–$0\overset{\rm p}{.}7$. We have reproduced these residual profiles by means of multiple-Gaussians fits. In Fig. 5 the integrated flux ($EW_{G_{N/B}}$), the $FWHM_N$, and the velocity shift ($\Delta V_{N/B}$) with respect to the center of stellar disk of the broad (circles) and narrow (dots) emission components, as well as of the extra-absorption (asterisks) are also displayed. The EW_{G_N} of the sharp core component is phase-dependent, with an amplitude smaller than the total Hα emission, $EW_{H\alpha}$. Moreover, its $FWHM_N$ is wider at the maximum emission, as observed for VY Ari. The radial velocity of the narrow emission component in the rest frame of the star center, ΔV_N, is always inside the $\pm v \sin i$ range. For the excess broad emission, observed only in a limited phase range, is hard to see any phase dependence. The extra-absorption

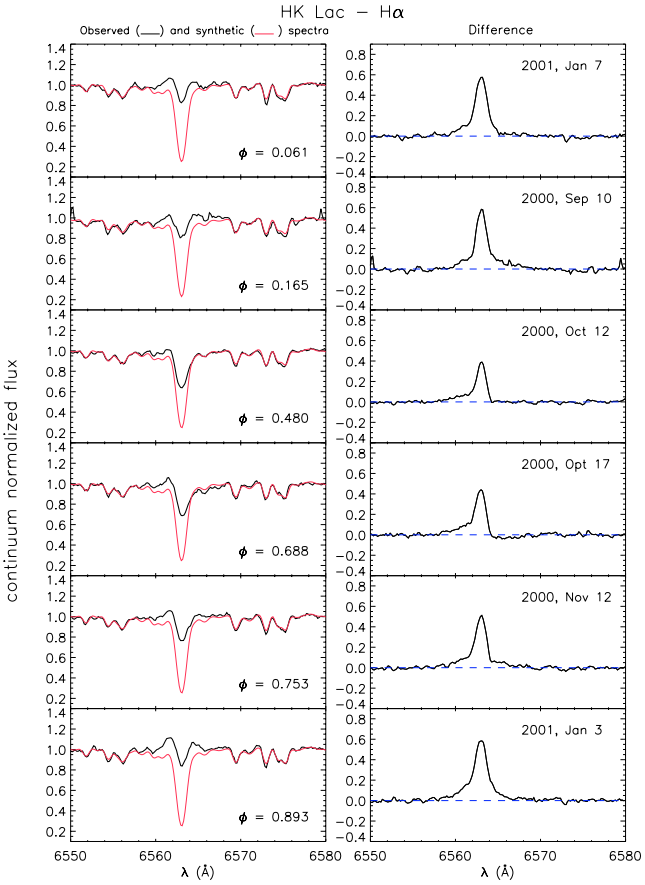

Fig. 6. *Left panels*: sample of observed and continuum-normalized spectra of HK Lac in the Hα region together with the non-active template. *Right panels*: difference between observed and template spectra.

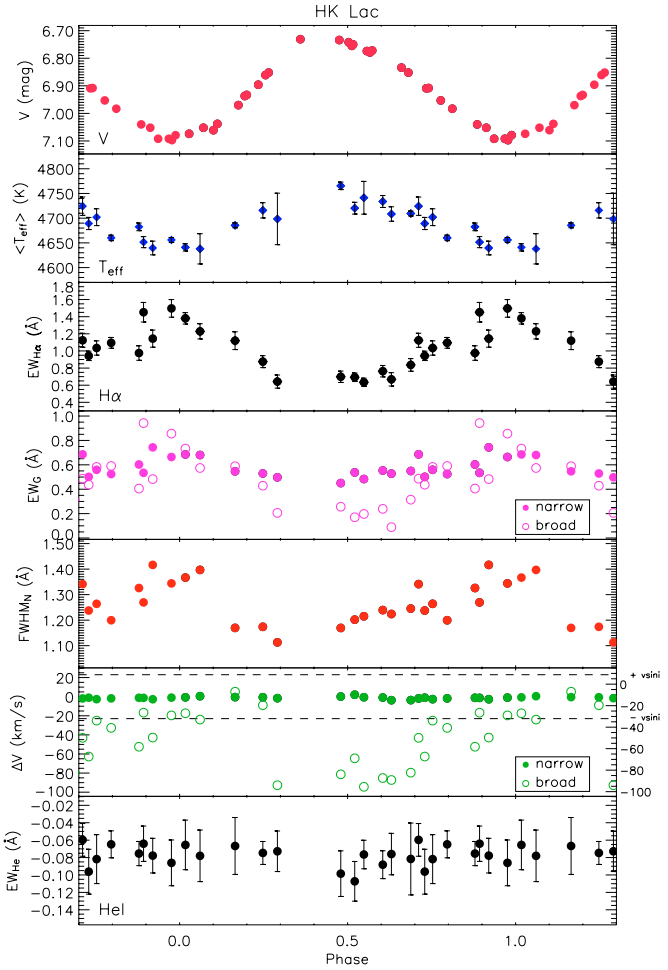

Fig. 7. *From top to bottom.* Johnson V photometry, average effective temperature, total Hα emission, equivalent width, $FWHM_{\rm N}$, relative radial velocity of the two-Gaussian fitting and He I D_3 equivalent width as a function of the rotational phase for HK Lac.

component displays a strong value at phase 0$^{\rm p}$.12 and progressively reduces its strength from 0$^{\rm p}$.40 till to disappear at phases greater than 0$^{\rm p}$.81. The equivalent width $EW_{\rm He}$ of helium line (lower panel in Fig. 5) shows also a scattered rotational modulation and a low value at the same phase of $EW_{\rm H\alpha}$ maximum extra-absorption.

The parameters of the difference spectra and the results of multiple-Gaussian fitting are listed in Table 2.

3.3. HK Lac

The spectra of HK Lac in the Hα region are displayed in Fig. 6 together with the spectrum of the adopted standard star ϵ Cyg (K0III) rotationally broadened to 23.0 km s^{-1} (Randich et al. 1994) with a linear limb-darkening coefficient μ_{6500} = 0.67 (Al-Naimiy 1978). The adopted rotational period is $P_{\rm rot}$ = 24.283 d (Paper II) and the initial Julian day is HJD$_{\phi=0}$ = 2 440 017.17 (Strassmeier et al. 1993b). The relevant emission in the Hα line with a highly variable intensity and shape is apparent. The Hα profile changes from a filled-in absorption ($\phi \simeq 0^{\rm p}.48$) to a double-peaked faint emission ($\phi \simeq 0^{\rm p}.89$), with spectra showing more emission in the blue Hα wing at intermediate phases. The total net equivalent width values are reported in Table 3 with the estimated errors and are plotted, as a function of phase, in Fig. 7.

This plot shows that the Hα maximum occurs at $\phi \simeq 0^{\rm p}.98$ and the Hα minimum is near to $\phi = 0^{\rm p}.55$, i.e. right at the same rotational phases as the minimum and the maximum of the temperature curve, respectively (Fig. 7). The anti-correlation of the Hα emission and the photospheric indicators in HK Lac has a remarkably specular behavior and is more striking than in the previous active stars. In analogy with the other stars, the temperature, brightness and Hα modulation curves display an asymmetric shape, implying at least two active regions (Paper II). This behavior is suggestive of a close spatial association of the photospheric and chromospheric active regions and was already observed in past seasons (Catalano et al. 1996; Frasca et al. 2002).

The reduced χ^2 is 2.3 for a Fourier polynomial fit to the $EW_{\rm H\alpha}$ curve of HK Lac, while it is 13.9 for a constant function. The probability $P_5(\chi^2)$ that a fit with 5 parameters gives a $\chi^2 \leq 2.3$ is of ≈20%, while, for $P_1(\chi^2)$, we obtain P = 99.98%, assuring a reliable statistical significance of the observed rotational modulation.

The rank-correlation coefficients found for HK Lac are $\rho = 0.909$ with a significance 7×10^{-8} for $V - T_{\rm eff}$, $\rho = -0.913$

Table 3. Parameters of the subtracted spectra of HK Lac.

HJD (+2 400 000)	Phase	$EW_{H\alpha}$ (Å)	$\Delta EW_{H\alpha}$ (Å)	EW_{G_N} (Å)	$FWHM_N$ (Å)	ΔV_N (km s^{-1})	EW_{G_B} (Å)	$FWHM_B$ (Å)	ΔV_B (km s^{-1})	EW_{He} (Å)	ΔEW_{He} (Å)
51 798.434	0.165	1.12	0.10	0.55	1.17	−0.5	0.59	3.97	5.2	−0.067	0.033
51 800.441	0.248	0.87	0.07	0.53	1.17	−0.6	0.43	6.18	−8.9	−0.075	0.013
51 801.492	0.291	0.64	0.08	0.50	1.11	−1.6	0.21	5.71	−92.7	−0.073	0.023
51 830.355	0.480	0.70	0.07	0.45	1.17	0.1	0.26	3.71	−81.3	−0.099	0.026
51 831.363	0.521	0.69	0.05	0.54	1.20	2.0	0.17	2.36	−64.6	−0.107	0.023
51 833.391	0.605	0.76	0.07	0.55	1.24	−0.9	0.24	3.04	−85.2	−0.088	0.016
51 835.414	0.688	0.84	0.07	0.55	1.25	−3.6	0.31	3.16	−79.6	−0.082	0.041
51 836.422	0.729	0.94	0.05	0.50	1.24	−1.1	0.44	2.73	−62.7	−0.096	0.026
51 856.309	0.548	0.63	0.05	0.48	1.22	−0.6	0.20	4.03	−94.4	−0.077	0.016
51 858.297	0.630	0.67	0.08	0.53	1.22	−3.7	0.09	2.07	−87.2	−0.076	0.024
51 860.262	0.711	1.12	0.08	0.69	1.34	−1.9	0.49	4.29	−43.1	−0.060	0.019
51 861.277	0.753	1.03	0.08	0.60	1.26	−2.6	0.58	5.25	−25.1	−0.082	0.028
51 862.328	0.796	1.09	0.06	0.52	1.20	−1.8	0.59	3.58	−32.7	−0.065	0.016
51 864.336	0.879	0.98	0.08	0.60	1.33	−1.2	0.41	2.99	−52.4	−0.075	0.014
51 865.332	0.920	1.14	0.10	0.74	1.42	−2.7	0.48	5.14	−42.8	−0.078	0.020
51 913.234	0.893	1.45	0.11	0.53	1.27	−1.2	0.94	4.08	−16.8	−0.064	0.020
51 915.250	0.976	1.50	0.10	0.66	1.34	−1.0	0.86	4.30	−19.6	−0.086	0.026
51 916.258	0.017	1.38	0.07	0.69	1.37	−0.7	0.73	4.21	−17.4	−0.066	0.029
51 917.316	0.061	1.23	0.09	0.68	1.40	0.5	0.57	3.94	−24.0	−0.078	0.030

with a significance 5×10^{-8} for V−Hα, $\rho = -0.762$ with a significance 2×10^{-4} for $T_{\rm eff}$−Hα. From the cross-correlation of the light curve and the Hα flux curve, we found a deep CCF minimum of −0.93 and a phase shift of $0\overset{p}{.}006$ that is not significantly different from zero, so that the two curves are nearly exactly anti-correlated. Similar results are obtained for the $T_{\rm eff}$–Hα CCF. These results are indicative of a very tight spatial association of photospheric and chromospheric ARs.

The residual Hα profiles of HK Lac have been also reproduced by means of narrow and broad Gaussian components. The equivalent width $EW_{G_{N/B}}$, the $FWHM_N$ and the velocity shift ΔV of these Gaussians components are displayed, as a function of the phase, in Fig. 7. For HK Lac the rotational modulation of the Hα intensity is observed in the $EW_{G_{N/B}}$ of both the narrow and broad components. The $FWHM_B$ of the broad component range from about 100 to 250 km s^{-1} without a specific trend with the phase, while the $FWHM_N$ of the narrow emission displays a nice rotational modulation in phase with its intensity (fifth box). Like for VY Ari, this could be indicative of stronger velocity fields and/or turbulent motions in ARs. The velocity shift ΔV_N of the narrow component is always inside the range ±23.0 km s^{-1}, the $v \sin i$ of HK Lac. The velocity with respect to the stellar disk center of the broader component is mainly blue-shifted and displays a strong variability with amplitude much larger than the rotational velocity. The minimum value $\Delta V_B \sim -90$ km s^{-1} is observed at phases from $0\overset{p}{.}3$ to $0\overset{p}{.}6$, i.e. in coincidence with the minimum Hα intensity. The maximum value $\Delta V_B \sim 0$ km s^{-1} is observed at $0\overset{p}{.}1$, just after the maximum $EW_{H\alpha}$. Different explanations can be given for this effect. For instance, an extended structure could be invoked. Another possibility could be that the chromospheric network is dominated by a blue-shifted emission coming from structures with outflow velocities (reminiscent of the solar spicules). When the active regions are facing the observer, the blue-shifted chromospheric network would be "overwhelmed" by broad but symmetrical Hα profile due to the chromospheric plages. A systematic blue-shift of the broad Hα emission component was observed by Zboril et al. (2004) in the very active RS CVn binary UZ Librae and explained in terms of velocity fields in the chromosphere.

He I D_3 absorption has been always detected, but no clear modulation emerges from the data scatter.

The parameters of the difference spectra and the results of multiple-Gaussian fitting are listed in Table 3.

4. Discussion

Each of the RS CVn systems studied in this work displays a particular Hα line behavior. VY Ari shows Hα profiles changing from double-peaked emission to filled-in absorption. This strong variation is typical of this star. Indeed, Bopp et al. (1989) found the Hα line varying from an emission feature above the continuum to a partially filled-in absorption one. They also report an occasionally enhanced a Hα emission presumably related to a transient flare event. Strassmeier et al. (1990) observed Hα emission feature ($EW_{H\alpha} = 0.947$ Å) with a strong and broad central reversal. Montes et al. (1995) found a weak Hα emission on the blue wing of a shallow absorption. As in our spectra in the phase range $0\overset{p}{.}7$–$1\overset{p}{.}0$, their residual Hα profiles display a remarkable blue-asymmetry suggesting a possible velocity field in the line formation region. Alekseev & Kozlova (2001) observed, the Hα line core always in

emission or strongly filled in. An absorption feature quite typical of K and M dwarf stars, which is attributed to self-absorption in an optically thick chromosphere, is observed at the line center. Moreover, some of the spectra presented by Alekseev & Kozlova (2001), taken in the same period of our observations, show both the Hα profiles and $EW_{\mathrm{H}\alpha}$ curve in good agreement with ours.

IM Peg displays a lower Hα intensity in agreement with past observations. Huenemoerder et al. (1990) observed a weakly variable Hα absorption line, whose intensity was possibly correlated with the orbital phase, and found a mean excess emission level $EW_{\mathrm{H}\alpha} = 0.99 \pm 0.20$ Å. They interpreted the Balmer emission as arising from globally distributed structures similar to the chromospheric network on the Sun or from nearly circumpolar regions. A highly variable Hα line, but with a lower mean value, was instead observed by Strassmeier et al. (1990) with $EW_{\mathrm{H}\alpha} = 0.00 \div 0.83$ Å. Frasca & Catalano (1994), from spectra taken at different orbital phases, but all within one cycle, found $EW_{\mathrm{H}\alpha} = 0.42 \div 0.67$ Å. Finally, Fernandez-Figueroa et al. (1994) found a slightly filled-in absorption Hα line.

For HK Lac several authors reported a variable Hα line. Bopp & Talcott (1980) found a Hα profile changing from filled-in absorption to weak double-peaked emission and to moderate single-peaked emission in spectra taken within a month. They proposed a speculative scenario in which the double-peaked Hα emission can be explained with a prominence-like feature that could give rise to flare eruptions. Liu & Tan (1986) observed an absorption profile with its blue wing in emission in all their observations. Catalano & Frasca (1994) found also a variable Hα profile mostly in emission, often with a double-peaked shape. They have also observed the complete development of a giant Hα flare lasting about six days and connected with a newly formed active region. They concluded that, in solar analogy, the flare eruption is produced by the interaction of new emerging magnetic flux with old magnetic structures. Fernandez-Figueroa et al. (1994) observed a weak emission in the red wing of the absorption line. Eker et al. (1995) found a very weak Hα absorption implying a relevant filling-in of the line core. Montes et al. (1997) observed a filled-in absorption Hα line with small variations during their observing run.

If we consider the phase behavior of the effective temperature and Hα emission for VY Ari, IM Peg and HK Lac in our observations, we note that the common outstanding characteristic is the striking anti-correlation, in the sense that the $EW_{\mathrm{H}\alpha}$ maximum is seen in correspondence with the T_{eff} minimum and the V light minimum. Anti-correlation between the optical light curve and the chromospheric or transition region line flux has been already reported for some active stars (Bopp & Talcott 1978; Ramsey & Nation 1984; Byrne et al. 1992; Rodonò 1987; Catalano et al. 1996; Frasca et al. 2000a; Alekseev & Kozlova 2001). In particular, Alekseev & Kozlova (2001) found that the brightness minimum of VY Ari, which corresponds to the maximum spot visibility, is accompanied by an increase in the Hα emission equivalent width. They noticed that such an enhancement is mainly due to the strengthening of the line intensity which, in the scheme of an isothermal chromosphere, implies an increase in the electron density. This supports the presence of chromospheric plages localized in the most heavily spotted hemisphere. For HK Lac, Frasca et al. (2002) found also an anti-correlation between Hα emission and light curves in their data collected from 1989 to 1997.

It is interesting to notice that the Hα variation amplitude does not seem to be correlated with the T_{eff} amplitude. For example, for VY Ari the $EW_{\mathrm{H}\alpha}$ variation factor is 2.5 and contemporaneously the hemisphere-averaged temperature varies by 3.6%. For IM Peg, instead, a similar relative temperature variation (2.6%) corresponds to a factor of about 10 in the $EW_{\mathrm{H}\alpha}$ variation. A similar behavior was already pointed out by Catalano et al. (1996) by comparing the Hα emission-curve amplitude with the V light-curve amplitude of some active RS CVn binaries.

The residual Hα profiles display in many cases broad wings that are sometimes blue- or red-shifted with respect to the central emission. These profiles have been well reproduced by a multiple-Gaussian fit with only two components, a narrow one for the line core and a broad one for the wings. Hatzes (1995) observed Hα spectra of DM UMa with similar shapes and suggested large-scale motions or winds in the chromosphere to explain the broad component. However, some authors (Montes et al. 1997) have interpreted the broad emission components observed in some RS CVn's and weak T Tauri stars as arising from microflaring. Indeed, these features are reminiscent of those observed during explosive events in the solar transition region, which are thought to be associated with emerging magnetic flux regions where field reconnection occurs. Microflares are frequent, short-duration, energetically weak disturbances, i.e. they lie in the low-energy tail of solar flare statistics. Their randomly distributed motions along the line of sight could explain the broad wings observed in the Hα and other chromospheric lines of very active stars (Montes et al. 1997). As a matter of fact, these authors find a good correlation between the contribution of the broad components and the degree of stellar activity. They also find that the larger changes in the excess Hα emission in their sample appear to occur predominantly in the broad component. It is well established that the Hα line become much broader during strong stellar flares (Foing et al. 1994; Montes et al. 1997).

We have observed, in all the three studied active stars, a clear modulation of the Hα emission that is essentially due to the narrow emission component. The $FWHM_{\mathrm{N}}$ of this component is also rotationally modulated, being larger when the emission is stronger. This could imply velocity fields and/or thermal effects in active regions stronger than in the quiet chromosphere.

5. Conclusion

In the present work we have simultaneously studied the rotational modulation of photospheric and chromospheric diagnostics in three magnetically active single-lined RS CVn stars, namely VY Ari, IM Peg and HK Lac.

We point out that, from the same data set at medium-resolution optical spectra, we have obtained information about the chromospheric and photospheric surface inhomogeneities

by using the Hα emission and the photospheric temperature (from line-depth ratios), respectively.

We have found, for all the observed stars, a tight anti-correlation between the Hα emission and the photospheric temperature modulations, that indicates a close spatial association between photospheric spots and chromospheric plages.

We have also fitted each individual Hα-emission profile with two Gaussians in order to obtain parameters such as equivalent widths of narrow and broad components, $FWHM$ and the velocity shifts with respect to the center of the stellar disk. We can conclude that the narrow component seems to be the principal responsible for the observed variations of the Hα equivalent width, with the exception of HK Lac where we found a significant modulation arising from both the narrow and the broad emission components.

Acknowledgements. The authors are grateful to an anonymous referee for a careful reading of the paper and valuable comments. This work has been supported by the Italian *Ministero dell'Istruzione, Università e Ricerca* (MIUR) and by the *Regione Sicilia* which are gratefully acknowledged. This research has made use of SIMBAD and VIZIER databases, operated at CDS, Strasbourg, France. We also want to thank Mrs. Luigia Santagati for the english revision of the text.

References

Alekseev, I. Y., & Kozlova, O. V. 2001, Astrophys., 44, 429
Al-Naimiy, H. M. 1978, Ap&SS, 53, 181
Barden, S. C. 1985, ApJ, 295, 162
Biazzo, K., Frasca, A., Henry, G. W., Catalano, S., & Marilli, E. 2005, in The 13th Cambridge Workshop on Cool Stars, Stellar Systems and the Sun, ed. F. Favata, ESA SP-560, 1, 445
Bopp, B. W., & Talcott, J. C. 1978, AJ, 83, 1517
Bopp, B. W., & Talcott, J. C. 1980, AJ, 85, 55
Bopp, B. W., Saar, S. H., Ambruster, C., et al. 1989, ApJ, 339, 1059
Byrne, P. B., Agnew, D. J., Cutispoto, G., et al. 1992, in Surface Inhomogeneities on Late-Type Stars, ed. P. B. Byrne, & D. J. Mullan (Berlin: Springer Verlag), 255
Catalano, S., & Frasca, A. 1994, A&A, 287, 575
Catalano, S., Rodonò, M., Frasca, A., & Cutispoto, G. 1996, in Stellar Surface Structure, ed. K. G. Strassmeier, & J. Linsky, IAU Symp., 176, 403
Catalano, S., Rodonò, M., Cutispoto, G., et al. 2000, in Variable Stars as Essential Astrophysical Tools, ed. C. İbanoğlu (Kluwer Academic Publishers), 687
Catalano, S., Biazzo, K., Frasca, A., & Marilli, E. 2002, A&A, 394, 1009 (Paper I)
De Medeiros, J. R., & Mayor, M. 1999, A&AS, 139, 433
Eker, Z., Hall, D. S., & Anderson, C. M. 1995, ApJS, 96, 581
Fernández-Figueroa, M. J., Montes, D., De Castro, E., & Cornide, M. 1994, ApJS, 90, 433
Foing, B. H., Char, S., Ayres, T., et al. 1994, A&A, 292, 543
Frasca, A., & Catalano, S. 1994, A&A, 284, 883
Frasca, A., Sanfilippo, D., & Catalano, S. 1996, A&A, 313, 532
Frasca, A., Catalano, S., & Mantovani, D. 1997, A&A, 320, 101
Frasca, A., Catalano, S., & Marilli, E. 1998, in The Tenth Cambridge Workshop on Cool Stars, Stellar Systems and the Sun, ed. J. A. Bookbinder, & R. A. Donahue (San Francisco: ASP), ASP Conf. Ser., 154, 1521
Frasca, A., Freire Ferrero, R., Marilli, E., & Catalano, S. 2000a, A&A, 364, 179
Frasca, A., Marino, G., Catalano, S., & Marilli, E. 2000b, A&A, 358, 1007
Frasca, A., Catalano, S., Marino, G., et al. 2002, in 1st Potsdam Thinkshop Poster Proc., 47
Frasca, A., Biazzo, K., Catalano, S., et al. 2005, A&A, 432, 647 (Paper II)
Freire Ferrero, R., Frasca, A., Marilli, E., & Catalano, S. 2004, A&A, 413, 657
Hall, J. C., & Ramsey, L. W. 1992, AJ, 104, 1942
Hatzes, A. P. 1995, ApJ, 109, 350
Herbig, G. H. 1985, ApJ, 289, 269
Huenemoerder, D. P., Ramsey, L. W., & Buzasi, D. L. 1990, ApJ, 350, 763
Kurucz, R. L. 1993, ATLAS9 Stellar Atmosphere Programs and 2 km s^{-1} grid, Kurucz CD-ROM No. 13
Lanzafame, A. C., Busà, I., & Rodonò, M. 2000, A&A, 362, 683
Lanzafame, A. C., & Byrne, P. B. 1995, A&A, 303, 155
Liu, X., & Tan, H. 1986, Chin. Astron. Astrophys., 10, 221
Montes, D., Fernández-Figueroa, M. J., De Castro, E., & Cornide, M. 1995, A&AS, 109, 135
Montes, D., Fernández-Figueroa, M. J., De Castro, E., & Sanz-Forcada, J. 1997, A&AS, 125, 263
Press, W. H., Flannery, B. P., Teukolsky, S. A., & Vetterling, W. T. 1986, Numerical Recipes. The Art of Scientific Computing (Cambridge University Press), 489
Ramsey, L. W., & Nation, H. L. 1984, AJ, 89, 115
Randich, S., Giampapa, M. S., & Pallavicini, R. 1994, A&A, 283, 893
Rodonò, M., Byrne, P. B., Neff, J. E., et al. 1987, A&A, 176, 267
Strassmeier, K. G., Fekel, F. C., Bopp, B. W., et al. 1990, ApJS, 72, 191
Strassmeier, K. G., Rice, J. B., Wehlau, W. H., et al. 1993a, A&A, 268, 671
Strassmeier, K. G., Hall, D. S., Fekel, F. C., & Scheck, M. 1993b, A&AS, 100, 173
Strassmeier, K. G., Bartus, J., Cutispoto, G., & Rodonò, M. 1997, A&AS, 125, 11
Zboril, M., Strassmeier, K. G., & Avrett, E. H. 2004, A&A, 421, 295
Zirin, H. 1988, Astrophysics of the Sun (Cambridge University Press), 351